Available online at www.sciencedirect.com
ScienceDirect
Polyhedron 27 (2008) 537–546
POLYHEDRON
www.elsevier.com/locate/poly

Crystal structures and physico-chemical properties of Zn(II) and Co(II) tetraaqua(3-nitro-4-hydroxybenzoato) complexes: Their anticonvulsant activities as well as related (5-nitrosalicylato)–metal complexes

Jean d'Angelo [a,*], Georges Morgant [a,*], Nour Eddine Ghermani [b,c], Didier Desmaële [a], Bernard Fraisse [c], François Bonhomme [b], Emma Dichi [d], Mehrez Sghaier [d], Yanling Li [e], Yves Journaux [e], John R.J. Sorenson [f,*]

[a] Laboratoire BioCIS, UMR CNRS 8076, IFR 141, Faculté de Pharmacie, Université Paris-Sud, 5 rue J.-B. Clément, 92296 Châtenay-Malabry, France
[b] Laboratoire PPB, UMR CNRS 8612, IFR 141, Faculté de Pharmacie, Université Paris-Sud, 5 rue J.-B. Clément, 92296 Châtenay-Malabry, France
[c] Laboratoire SPMS, UMR CNRS 8580, Ecole Centrale Paris, Grande Voie des Vignes, 92295 Châtenay-Malabry, France
[d] Laboratoire CPMB, Faculté de Pharmacie, Université Paris-Sud, 5 rue J.-B. Clément, 92296 Châtenay-Malabry, France
[e] Laboratoire CIMM, UMR CNRS 7071, Université Pierre et Marie Curie Paris 6, 4 Place Jussieu, 75005 Paris, France
[f] Division of Medicinal Chemistry, Department of Pharmaceutical Sciences, University of Arkansas, Medical Sciences Campus, Slot 522, 4301 West Markham Street, Little Rock, AR 72205, USA

Received 4 September 2007; accepted 4 October 2007
Available online 14 November 2007

Abstract

Purposes of these studies were to synthesize Zn(II) and Co(II) complexes of 3-nitro-4-hydroxybenzoic acid, determine their structures through X-ray crystallography, and obtain their anticonvulsant activities. Thermogravimetric, differential scanning calorimetry, impedance of aqueous solutions and magnetic properties analyses were also determined. Anticonvulsant and related activities of these complexes as well as Zn(II), Co(II), Ni(II) and Mg(II) (5-nitrosalicylato) complexes were determined by the National Institutes of Health, Antiepileptic Development Program. Results of these analyses are presented to document unique bonding features and physical properties of these compounds and their anticonvulsant activities. It is concluded that these compounds have chemical and physical properties that can be used to account for their anticonvulsant activities.

Keywords: Crystal structures; 3-Nitro-4-hydroxybenzoic acid ligand; Zn(II) and Co(II) complexes; Anticonvulsant activity

1. Introduction

Besides their relevance to solid state structure and supramolecular design [1–3], (salicylato)–metal complexes have attracted considerable attention, because of their promising anti-inflammatory and anticonvulsant activities [4–10]. As part of a systematic program devoted to the study of structure–activity relationships of (salicylato)–metal complexes, we recently reported the preparation and crystal structures of (5-nitrosalicylato) complexes of Mg(II), Zn(II), Co(II) and Ni(II). The building units of these complexes self-assemble via π–π stacking and extensive intermolecular hydrogen bonding, resulting in a 3D supramolecular architecture [5]. Although the 5-nitrosalicylate ligand, 5-nsa, has a very versatile coordination behavior, an exciting feature in this series is the possibility of modifying the original structure by moving groups attached to the aromatic nucleus. By shifting the hydroxyl group from C-2 to the C-4 position of the 5-nsa ligand, a

* Corresponding authors. Tel.: +33 146835699; fax: +33 146835752 (J. d'Angelo); tel.: +33 146835463 (G. Morgant); tel.: +1 501 686 6494; fax: +1 501 526 6510 (J.R.J. Sorenson).
E-mail addresses: jean.dangelo@u-psud.fr (J. d'Angelo), georges.morgant@u-psud.fr (G. Morgant), sorensonjohnrj@uams.edu (J.R.J. Sorenson).

0277-5387/$ - see front matter © 2007 Elsevier Ltd. All rights reserved.
doi:10.1016/j.poly.2007.10.006

suitable set of ligands for intermolecular anchoring through hydrogen bonding was thus obtained for our intended evaluations.

Herein we report the crystal structures of (3-nitro-4-hydroxybenzoato) complexes of Zn(II) and Co(II). A key aspect of these structures is that the individual units self-assemble via extensive hydrogen bonding, leading to an original 3D continuum. Although, in the strict sense, the present complexes are not salicylate derivatives but 4-OH regioisomers, their anticonvulsant properties were determined to examine the effect of this structural change on the structural and physical properties of these complexes in relation to their pharmacological effects. For the sake of comparison, the anticonvulsant activities of related transition metalloelement 5-nsa complexes were also determined [5]. Interestingly, promising pharmacological responses were obtained for these complexes as anticonvulsants. Critical to the knowledge of the mode of action of present anticonvulsant metal complexes was the identification of the actual pharmacologically active entity that crosses the blood–brain barrier. Toward this end, this report presents: (1) the conducting properties of the metal complexes in dilute aqueous solution and (2) water/1-octanol extraction experiments which revealed an unexpected equilibrium between these complexes and the corresponding free ligands.

2. Experimental

2.1. Materials

High purity 3-nitro-4-hydroxybenzoic acid, zinc sulfate heptahydrate and cobalt sulfate heptahydrate were purchased from Acros (USA) and used without further purification.

2.2. Physical measurements

Elemental analyses (C, H and N) were performed with a Perkin–Elmer 2400 analyzer. Infrared spectra were recorded with a Bruker Vector 22 spectrometer. Thermogravimetric analyses (TGA) were performed with a TA Instruments TGA Q500 apparatus. Calibrations were performed at different temperatures using Curie magnetic transitions for the recommended materials: alumel (163 °C) and nickel (354 °C). Mass calibrations were performed using a standard mass of 100 mg. The furnace was calibrated between 100 and 900 °C to verify thermocouple performance. All experiments were performed under dry nitrogen, with a flow rate of 6×10^{-2} l min^{-1}. Analysis of compounds following nitrogen purging was conducted using a heating rate of 20 °C min^{-1} in order to determine percent mass loss with optimal precision. Differential Scanning Calorimetry (DSC) experiments were performed with a TA Instruments Universal V4.2E apparatus under nitrogen. Samples were introduced in aluminum pans and covered with holed caps in view to avoid uncontrolled variation of pressure. Calibration of temperature was performed with 5 N quality indium at 156.6 °C and tin at 231.9 °C and a heating rate of 10 °C min^{-1}. Impedance measurements of aqueous solutions were performed using a VoltaLab 80 (Radiometer Analytical) with a 2-pole cell with two platinum plates. The signal amplitude was 100 mV. A continuous potential of 0 mV was imposed. Solutions, preserved under nitrogen, were placed in a double walled glass cell ensuring thermal stabilization. Measurements were obtained at 20 °C. Magnetic measurements in the 2–300 K temperature range were carried out with a MPMS5 SQUID susceptometer (Quantum Design Inc.).

2.3. Synthesis of complexes

2.3.1. $C_{14}H_{16}N_2O_{14}Zn$ (**1**)

Sodium 3-nitro-4-hydroxybenzoate was prepared by neutralizing 3-nitro-4-hydroxybenzoic acid (0.915 g, 5 mmol) with 5 ml of 1 M NaOH in deionized water. To this solution was added $ZnSO_4 \cdot 7H_2O$ (0.720 g, 2.5 mmol) in 3 ml of water. After a few days **1** was filtered, crystallized from water, and dried over anhydrous magnesium sulfate. Yield: 0.939 g (75%). *Anal.* Calc. for $C_{14}H_{16}N_2O_{14}Zn$ (**1**): C, 33.52; H, 3.21; N, 5.58. Found: C, 33.43; H, 3.18; N, 5.56%. IR (neat, cm^{-1}): 3254 (s), 1621 (s), 1587 (s), 1526 (s), 1420 (s), 1379 (s), 1323 (s), 1264 (s), 1178 (s), 1153 (s), 1118 (s), 1074 (s), 942 (m), 916 (m), 858 (m), 825 (m), 789 (s), 764 (s), 684 (s), 638 (s).

2.3.2. $C_{14}H_{16}N_2O_{14}Co$ (**2**)

Sodium 3-nitro-4-hydroxybenzoate was prepared by neutralizing 3-nitro-4-hydroxybenzoic acid (0.915 g, 5 mmol) with 5 ml of 1 M NaOH in deionized water. To this solution was added $CoSO_4 \cdot 7H_2O$ (0.702 g, 2.5 mmol) in 3 ml of water. After a few days **2** was filtered, crystallized from water, and dried over anhydrous magnesium sulfate. Yield: 0.943 g (76%). *Anal.* Calc. for $C_{14}H_{16}N_2O_{14}Co$ (**2**): C, 33.95; H, 3.25; N, 5.66. Found: C, 34.05; H, 3.18; N, 5.64%. IR (neat, cm^{-1}): 3259 (m), 1621 (s), 1586 (s), 1545 (s), 1524 (s), 1418 (s), 1381 (s), 1323 (s), 1264 (s), 1179 (s), 1153 (s), 1117 (s), 1073 (m), 938 (m), 915 (m), 859 (m), 825 (m), 807 (s), 789 (s), 763 (s), 685 (s), 638 (s).

2.4. X-ray diffraction measurements

Diffraction data were collected with a Bruker-SMART three axis diffractometer equipped with a SMART 1000 CCD area detector using graphite monochromated Mo Kα X-radiation (wavelength $\lambda = 0.71073$ Å) at 100.0(1) K. The low temperature was reached by an evaporated liquid nitrogen stream over the crystal, provided by the Oxford Cryosystem device. Data collection and processing were performed using Bruker SMART programs [11] and empirical absorption correction was applied using SADABS computer program [11]. The structure was solved by direct methods using SIR97 [12], and refined by full-matrix least-

Table 1
Crystal data and structure refinement parameters for $C_{14}H_{16}N_2O_{14}M$ (**1**, M = Zn and for **2**, M = Co)

Compound	1	2
Empirical formula	$C_{14}H_{16}N_2O_{14}Zn$	$C_{14}H_{16}N_2O_{14}Co$
Molecular weight	501.67	495.22
Color	yellowish	pink
Crystal system	triclinic	triclinic
Space group	$P\bar{1}$	$P\bar{1}$
a (Å)	6.209(5)	6.197(5)
b (Å)	10.071(5)	5.047(5)
c (Å)	14.729(5)	14.671(5)
α (°)	83.579(5)	83.992(5)
β (°)	79.084(5)	99.698(5)
γ (°)	89.427(5)	89.944(5)
V (Å^3)	898.6(9)	449.5(6)
Z	2	1
D_{calc} (g cm^{-3})	1.854	1.829
Absorption coefficient (mm^{-1})	1.452	1.040
$F(000)$	512	253
Crystal size (mm)	$0.17 \times 0.22 \times 0.27$	$0.18 \times 0.22 \times 0.25$
θ Ranges (°)	1.42–29.78	2.83–29.54
$h/k/l$	−8, 8/−13, 13/0, 19	−6, 6/−8, 7/0, 19
T (K)	100	100
Number of reflections collected	6383	3064
Number of reflections used $\geqslant 3\sigma(I)$	4266	1834
Parameters	281	142
R [F^2]	0.0243	0.0346
wR [F^2]	0.0581	0.0821
Goodness-of-fit on F^2	0.9011	0.8934
Residual density (e Å^{-3})	−0.64; 0.64	−0.51; 0.58
Refine ls shift/su.max	0.0019	0.0003

squares based on F^2 using CRYSTALS software [13]. The molecule was drawn using the CAMERON program [14]. All non-hydrogen atoms were anisotropically refined. Hydrogen atoms were located in difference Fourier maps. H atoms were refined isotropically with $U_{iso} = 1.20U_{eq}$ where U_{eq} is the equivalent isotropic atomic displacement parameter of the attached atom. Crystal parameters, data collection and the refinement details of compounds **1** and **2** are reported in Table 1.

2.5. Determination of anticonvulsant activities and Rotorod toxicity

Anticonvulsant activities and Rotorod toxicity of $C_{14}H_{16}N_2O_{14}Zn$ (**1**) and $C_{14}H_{16}N_2O_{14}Co$ (**2**), as well as previously reported related complexes **3**–**6** [5], were determined by the National Institute of Health-National Institute of Neurological Disorders and Stroke-Antiepileptic Drug Development program for the detection and evaluation of compounds as anticonvulsant agents (USA). *Maximal electroshock seizure* were elicited with a 60 cycle alternating current of 50 mA, five to seven times that necessary to elicit minimal electroshock seizures, delivered for 0.2 s via corneal electrodes. *Psychomotor seizures test*: the delivery of a less intense electric stimulation, which produces less intense brain inflammation, via corneal electrodes of 6 Hz, 44 mA or lower, for 3 s is used to produce psychomotor seizures, following instillation of a drop of 0.9% saline prior to this application of electric current. Abolition of the visual stereotypic behavior characterized as minimal clonic automatistic behaviors. *Subcutaneous* (*sc*) *pentylenetetrazol* (*Metrazol*) *seizure threshold test*: a dose of pentylenetetrazol, a potent CNS stimulant (Central Nervous System), which produces seizures in greater than 97% of treated mice, 85 mg/kg of body mass, was administered sc as a 0.5% solution in saline at the posterior neck midline. Animals were observed for 30 min. Failure to observe even a threshold seizure, a single episode of clonic spasms of at least 5 s duration, is defined as anticonvulsant activity. *Rotating rod test*: mice or rats are placed on a 1 inch diameter knurled plastic rod rotating at six revolutions per min. Normal mice and rats can remain on a rod rotating at this speed indefinitely. Neurologic toxicity, either CNS stimulation or depression, is evidenced by a failure of the mouse or rat to remain on the rotating rod for 1 min.

3. Results and discussion

3.1. Description of the $C_{14}H_{16}N_2O_{14}Zn$ (**1**) and $C_{14}H_{16}N_2O_{14}Co$ (**2**) structures based upon X-ray crystallography

Complexes **1** and **2** can be represented by the general formula $(C_7H_4NO_5)_2M(H_2O)_4$, where $M = Zn^{II}$ or Co^{II}. The canonical drawings of these complexes are represented in Fig. 1 and the CAMERON molecular structures in Figs. 2 and 3, with the atom numbering system used in Table 2 which lists the most relevant bond distances and angles.

The formula units of complexes **1** and **2** can be represented by $(C_7H_4NO_5)_2M(H_2O)_4$ where M = Zn or Co. For complex **2**, the asymmetric unit consists of the half of formula unit. In both complexes, the coordination octahedron around the metal atom involves one carboxylato O-atom from each 3-nitro-4-hydroxybenzoate ligand (acting as a monodentate linker) and the O-atoms of the four water molecules harnessed to the metal atom. In $(C_7H_4NO_5)_2Zn(H_2O)_4$ (**1**), the octahedron is slightly distorted. The *cis* angles around the Zn center vary between 85.97(7)° and 92.95(7)° while the *trans* angles vary from 175.70(5)° to 178.68(5)°. The Zn–O(26) and Zn–O(36) distances, 2.074(2) and 2.052(2) Å, respectively, are notably shorter than those for Zn–O(10), Zn–O(11), Zn–O(12), and Zn–O(13); 2.186(2), 2.114(2), 2.092(2), and 2.118(2) Å, respectively.

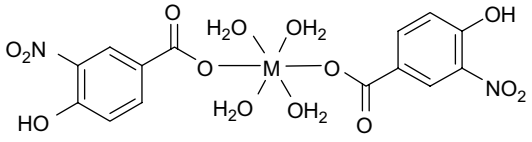

Fig. 1. Canonical representation of $(C_7H_4NO_5)_2M(H_2O)_4$ (**1**, M = Zn; **2**, M = Co).

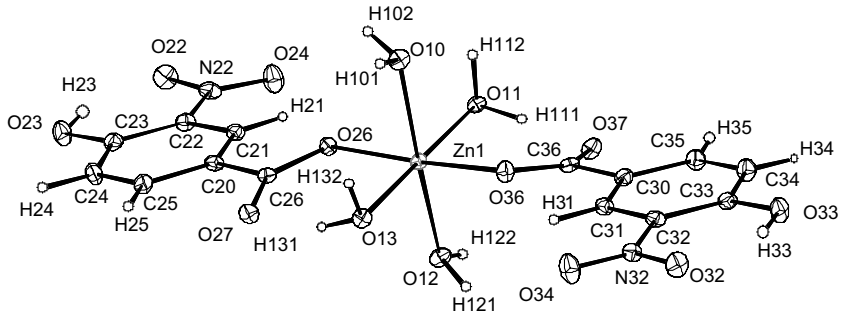

Fig. 2. Labeled CAMERON diagram of $(C_7H_4NO_5)_2Zn(H_2O)_4$ (**1**). Ellipsoids are drawn at a 50% probability level.

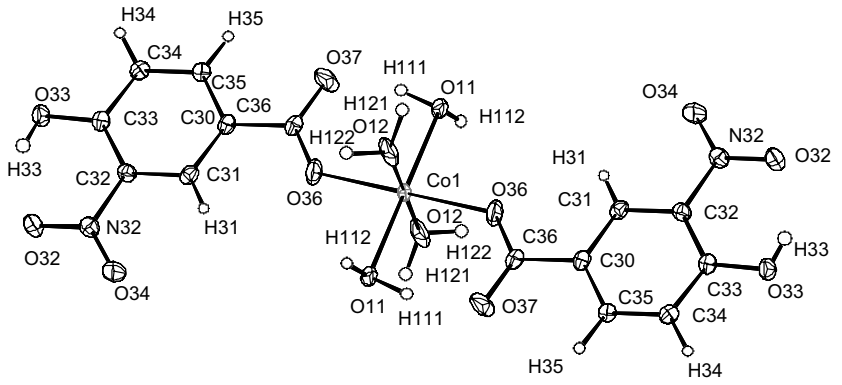

Fig. 3. Labeled CAMERON diagram of $(C_7H_4NO_5)_2Co(H_2O)_4$ (**2**). Ellipsoids are drawn at a 50% probability level.

In contrast, the structure of $(C_7H_4NO_5)_2Co(H_2O)_4$ (**2**) consists of centrosymmetric monomers with the metal atom occupying the inversion center at 0, 1/2, 1/2 of the triclinic unit cell. This symmetry is revealed by two identical metal–carboxylato O-atom lengths of 2.070(2) Å and two pairs of metal–O (water) distances of 2.100(2) and 2.070(2) Å. On the other hand, the *cis* angles around the Co center consist of six centrosymmetrically-related pairs, while identical values were observed for the three *trans* angles, 180.00(8)°. Since complexes **1** and **2** exhibit very close structural features, only details of the packing in **1** were arbitrarily chosen for presentation and discussion in the present paper. The presence of four water molecules around the metal center led to a very extensive and complicated H-bonding network. A list of the most probable atoms involved in H-bonds with their related angles is given in Tables 3 and 4. Fig. 4 shows the H-bonding in **1** around the Zn center. The crystal cohesion is thus ensured by fourteen hydrogen bonds per formula unit.

The individual zero-dimensional units (0D) of **1** are linked together through intermolecular hydrogen bonding implying their *ortho*-nitrophenol groups ends, $O(23)^{iv}$–$H(23)^{iv}\cdots O(32)$ and $O(33)$–$H(33)\cdots O(22)^{iv}$ forming infinite 1D chains (Figs. 5 and 6). The intrachain separation of the Zn centers is 18.82 Å (18.85 Å for Co–Co in complex **2**). It is noteworthy that the *ortho*-nitrophenol groups are also implied in intramolecular hydrogen bonding, $O(23)^{iv}$–$H(23)^{iv}\cdots O(22)^{iv}$ and $O(33)$–$H(33)\cdots O(32)$, which clearly reinforces the cohesion of these chains.

Table 2
Selected bond distances (Å) and bond angles (°) for $(C_7H_4NO_5)_2Zn(H_2O)_4$ (**1**) and $(C_7H_4NO_5)_2Co(H_2O)_4$ (**2**)

1		**2**	
Bond lengths		*Bond lengths*	
Zn–O(10)	2.186(2)	Co–O(11)	2.127(2)
Zn–O(11)	2.114(2)	Co–O(12)	2.100(2)
Zn–O(12)	2.092(2)	Co–O(36)	2.070(2)
Zn–O(13)	2.118(2)		
Zn–O(26)	2.074(2)		
Zn–O(36)	2.059(2)		
Bond angles		*Bond angles*	
O(10)–Zn–O(12)	177.58(6)	$O(11)^{vi}$–Co–O(11)	180.00(8)
O(11)–Zn–O(13)	178.68(5)	$O(12)^{vi}$–Co–O(12)	180.00(8)
O(26)–Zn–O(36)	175.70(5)	$O(36)^{vi}$–Co–O(36)	180.00(8)
O(10)–Zn–O(11)	86.57(6)	$O(11)^{vi}$–Co–$O(36)^{vi}$	93.26(8)
O(10)–Zn–O(13)	92.61(6)	O(11)–Co–O(36)	93.26(8)
O(10)–Zn–O(26)	89.03(6)	$O(11)^{vi}$–Co–$O(12)^{vi}$	88.40(9)
O(10)–Zn–O(36)	86.98(6)	O(11)–Co–O(12)	88.40(9)
O(12)–Zn–O(11)	91.03(7)	$O(12)^{vi}$–Co–O(11)	91.60(9)
O(12)–Zn–O(13)	89.78(6)	$O(11)^{vi}$–Co–O(12)	91.60(9)
O(12)–Zn–O(26)	91.21(6)	$O(36)^{vi}$–Co–O(12)	89.68(9)
O(12)–Zn–O(36)	92.84(6)	$O(12)^{vi}$–Co–O(36)	89.68(9)
O(11)–Zn–O(26)	88.42(7)	$O(11)^{vi}$–Co–O(36)	86.74(8)
O(11)–Zn–O(36)	92.95(7)	$O(36)^{vi}$–Co–O(11)	86.74(8)
O(13)–Zn–O(26)	92.60(7)	$O(12)^{vi}$–Co–$O(36)^{vi}$	90.32(9)
O(13)–Zn–O(36)	85.97(7)	O(12)–Co–O(36)	90.32(9)

Symmetry code: ^{vi} $-x, -y+1, -z+1$.

The parallel chains are further engaged in hydrogen bonding implying H(102), H(112) and H(121) with interchain separations of 4.904 Å and 5.200 Å (5.047 Å for com-

Table 3
H-bond donor/acceptor scheme (Å, °) for $(C_7H_4NO_5)_2Zn(H_2O)_4$ (**1**)

D–H···A	*d*(D–H)	*D*(H···A)	∠(DHA)
O(23)–H(23)···O(22)	0.795(2)	1.865(2)	153.13(9)
O(33)–H(33)···O(32)	0.815(2)	1.902(2)	143.30(9)
O(11)–H(111)···O(37)	0.940(2)	1.714(2)	161.11(9)
O(13)–H(131)···O(27)	0.940(2)	1.720(2)	160.63(8)
O(10)–H(101)···O(37)^{i}	0.934(2)	1.939(2)	147.17(9)
O(13)–H(132)···O(37)^{i}	0.940(2)	1.769(2)	164.39(9)
O(12)–H(122)···O(27)^{ii}	0.932(2)	1.912(2)	166.64(9)
O(11)–H(112)···O(26)^{iii}	0.939(2)	1.779(2)	166.97(8)
O(10)–H(102)···O(11)^{iii}	0.936(2)	1.938(2)	154.65(8)
O(33)–H(33)···O(22)^{iv}	0.814(2)	2.345(2)	139.78(9)
O(23)^{iv}–H(23)^{iv}···O(32)	0.794(2)	2.401(2)	130.98(9)
O(23)–H(23)···O(32)^{v}	0.794(2)	2.401(2)	130.98(9)
O(33)^{v}–H(33)^{v}···O(22)	0.814(2)	2.345(2)	139.78(9)
O(12)–H(121)···O(13)^{vi}	0.927(2)	1.888(2)	174.50(8)

Symmetry codes: ^{i} $x+1, y, z$; ^{ii} $x-1, y+z$; ^{iii} $-x, -y, -z+1$; ^{iv} $x-1, y+1, z+1$; ^{v} $x+1, y-1, z-1$; ^{vi} $-x, -y+1, -z+1$.

Table 4
H-bond donor/acceptor scheme (Å, °) for $(C_7H_4NO_5)_2Co(H_2O)_4$ (**2**)

D–H···A	*d*(D–H)	*D*(H···A)	∠(DHA)
O(11)–H(111)···O(37)	0.954(4)	1.673(2)	163.01(8)
O(11)–H(112)···O(36)^{i}	0.951(7)	2.162(3)	158.83(6)
O(12)–H(122)···O(11)^{ii}	0.944(7)	1.860(3)	170.02(9)
O(12)–H(121)···O(37)^{iii}	0.947(5)	1.834(3)	161.37(9)
O(33)–H(33)···O(32)	0.810(5)	1.898(3)	144.75(6)
O(33)–H(33)···O(32)^{iv}	0.810(5)	2.346(2)	138.38(5)
O(33)^{iv}–H(33)^{iv}···O(32)	0.810(5)	2.346(2)	138.38(5)

Symmetry codes: ^{i} $x+1, y, z$; ^{ii} $x, y-1, z$; ^{iii} $-x+1, -y+1, -z+1$; ^{iv} $-x-2, -y+2, -z+2$.

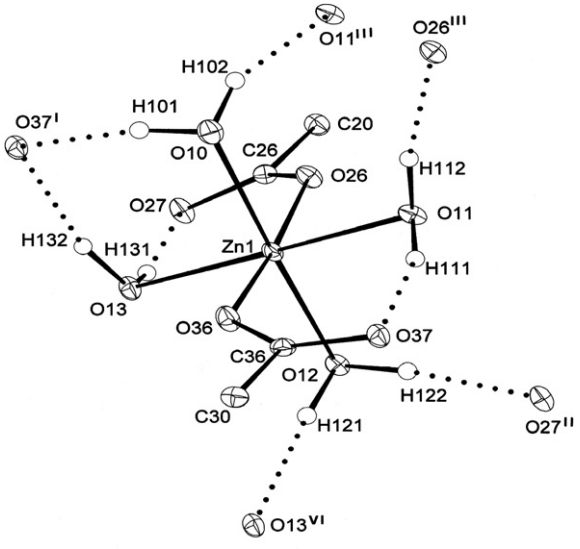

Fig. 4. Labeled diagram of $(C_7H_4NO_5)_2Zn(H_2O)_4$ (**1**) focusing on the hydrogen bonding system around the Zn atom (dashed lines).

plex **2**) resulting in 2D sheets (Fig. 7). These, in turn, self-assemble via hydrogen bonds implying H(122) and H(132) with an interplanar separation of 6.209 Å (7.996 Å for complex **2**) yielding a 3D supramolecular architecture (Fig. 8).

One of the most salient features of this architecture is the compact 3D arrangement of the metal atoms. In complex **1**, the Zn atoms are close to each other, with distances of 4.904, 5.200 and 6.209 Å (Fig. 9a). A centrosymmetric metal arrangement pattern was observed for complex **2** with Co – Co distances of 5.047 and 6.197 Å (Fig. 9b).

3.2. Thermal analysis: TGA and DSC measurements

TGA analysis of **1** revealed a mass loss of 14.8% on heating from 50 to 180 °C, corresponding to a loss of four crystalline water molecules (Calc. 14.4%). TGA analysis of **2** revealed a mass loss of 15.1% on heating from 80 to 180 °C, corresponding to a loss of four crystalline water molecules (Calc. 14.5%). On heating **2** from 80 to 550 °C, an overall mass loss of 85.5% was observed. The non-volatile residue, 14.5% of the starting material, corresponds to one molecule of CoO (Calc. 15.1%). The DSC study of **1** revealed, as the main event, a narrow endotherm centered at 141 °C corresponding to loss of water and a narrow exotherm centered at 342 °C. A similar thermal pattern was observed for complex **2**, with an endotherm centered at 130 °C and exotherm centered at 349 °C.

3.3. Electrochemical impedance measurements

The electrochemical impedance $Z(\omega)$ of the studied sample between the two plates of the conductivity cell is a complex number which can be represented, in polar coordinates by its module $|Z|$ and its phase, in Cartesian representations by its real part Z' and its imaginary part Z'' with $Z(\omega) = Z' + i\,Z''$. At the time of frequency scanning, the experimental points were distributed on a curve having the form of an arc of a circle. The obtained curve is called a Nyquist diagram ($-Z''$ versus Z'). Z'_1 to high frequency, HF, and Z'_2 to low frequency, LF, are the impedance when 'Z' crosses the OZ axis (real axis). The Nyquist curves for 1×10^{-4} M solutions of complexes **1** and **2** (a concentration close to the doses administered in the anticonvulsant and toxicity assays, see Section 3.6) are shown in Fig. 10. The existence of a half circle is typical of the presence of a simple charge transfer. Table 5 gives the electrochemical conductances $(1/Z')$ of complexes **1** and **2** at concentrations of 1×10^{-4} M and 5×10^{-4} M in deionized water. At LF, conductances $(1/Z'_2)$ of solutions of complexes **1** and **2** at identical concentrations are very similar (compare entries 1 and 5 in one hand, and 3 and 7 in the other hand). These values are notably higher than the conductance of deionized water employed in the present experiments (entry 9), that is to say, approximately 25 times for a concentration of 1×10^{-4} M and 130 times for a concentration of 5×10^{-4} M. Note that at LF, the cell capacitance is assumed to be so small that it may be neglected. However, at HF, conductances $(1/Z'_1)$ for solutions of both complexes are of the same order of magnitude, irrespective of

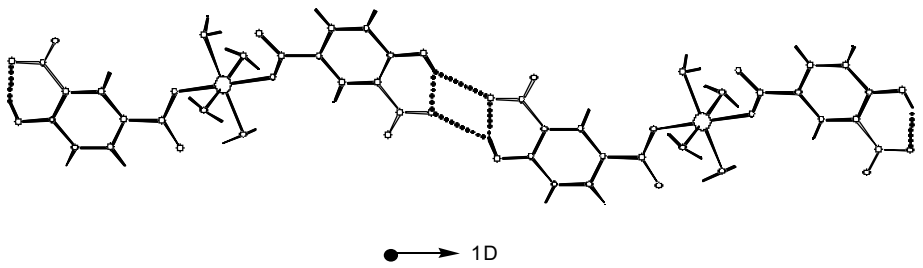

Fig. 5. Part of $[(C_7H_4NO_5)_2Zn(H_2O)_4]_n$ (**1**)$_n$ showing the 1D chain structure with intrachain hydrogen bonds (dashed lines). Zn centers are symbolized by large circles.

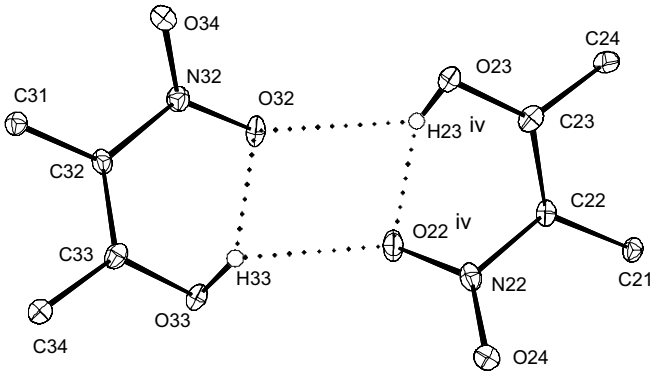

Fig. 6. Labeled diagram of $(C_7H_4NO_5)_2Zn(H_2O)_4$ (**1**) focusing on the hydrogen bonding system around the *ortho*-nitrophenol groups (dashed lines).

concentrations of these complexes (entries 2, 4, 6 and 8), and close to that of deionized water (entry 10). Clearly, at HF, the cell capacitance now markedly competes with the cell resistance, leading to fatal errors in conductance measurements. LF measurements indicate that the conductances of the 1×10^{-4} M and 5×10^{-4} M complex solutions do not differ greatly from those of KCl solutions at these concentrations (entries 11 and 12). Complexes **1** and **2** are therefore strong electrolytes.

3.4. Magnetic measurements

The magnetic properties of Co-complex **2** are shown in Fig. 11. At room temperature, $\chi_M T$ is equal to 3.02 cm^3 K mol^{-1}, value expected for an isolated Co(II) ion. Upon cooling, the $\chi_M T$ values steadily decrease up to 7 K. Below this temperature, the decrease of $\chi_M T$ is steeper to reach a value of 1.62 cm^3 K mol^{-1} at 2 K. In fact, in the 300–30 K temperature range, the experimental curve can be fitted using the theoretical behavior of a distorted octahedral isolated cobalt ion [15]. The best fit of the data by full-matrix diagonalization of the appropriate spin Hamiltonian is obtained with the following parameter $\lambda = -117$, $D = 605$ and $\kappa = 1$ where λ, D and κ stand for spin–orbit constant, axial distortion and orbital reduction factor, respectively. As shown in the inset of Fig. 11, below 30 K the experimental data deviate from the theoretical curve. First, between 30 and 3 K the experimental data are above the theoretical curve indicating that ferromagnetic interaction between Co ions is operative within the

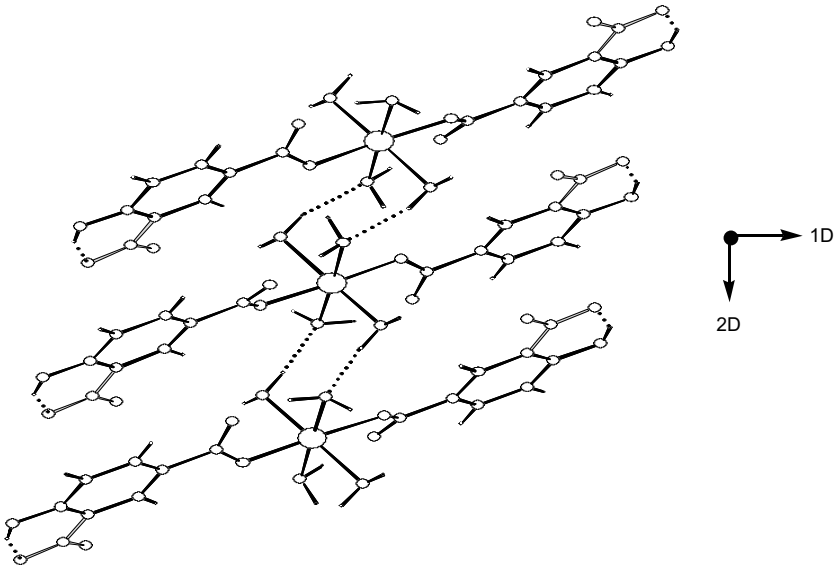

Fig. 7. Packing of $(C_7H_4NO_5)_2Zn(H_2O)_4$ (**1**) showing the H-bonded 2D continuum as dashed lines. Zn centers are symbolized by large circles.

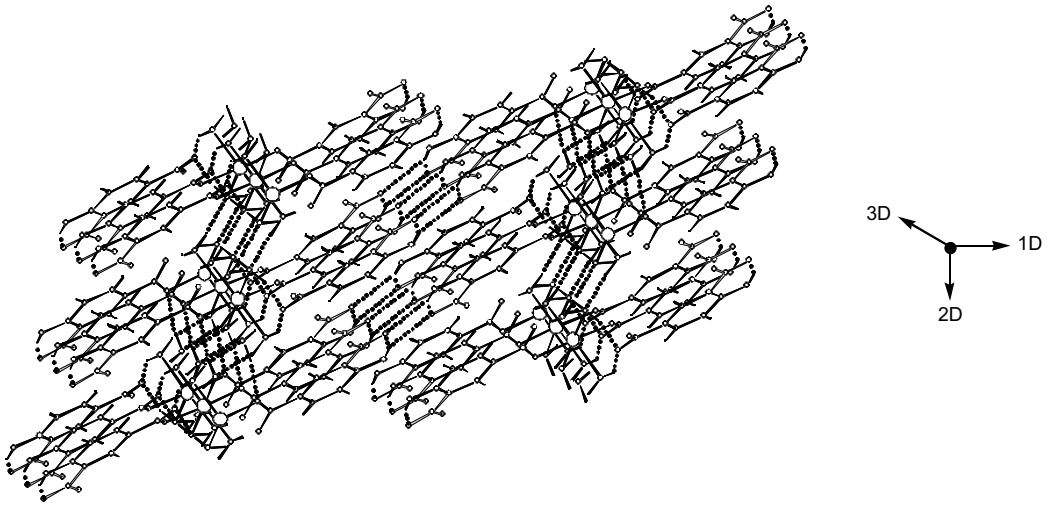

Fig. 8. Packing of $(C_7H_4NO_5)_2Zn(H_2O)_4$ (**1**) showing the H-bonded 3D continuum as dashed lines. Zn centers are symbolized by large circles.

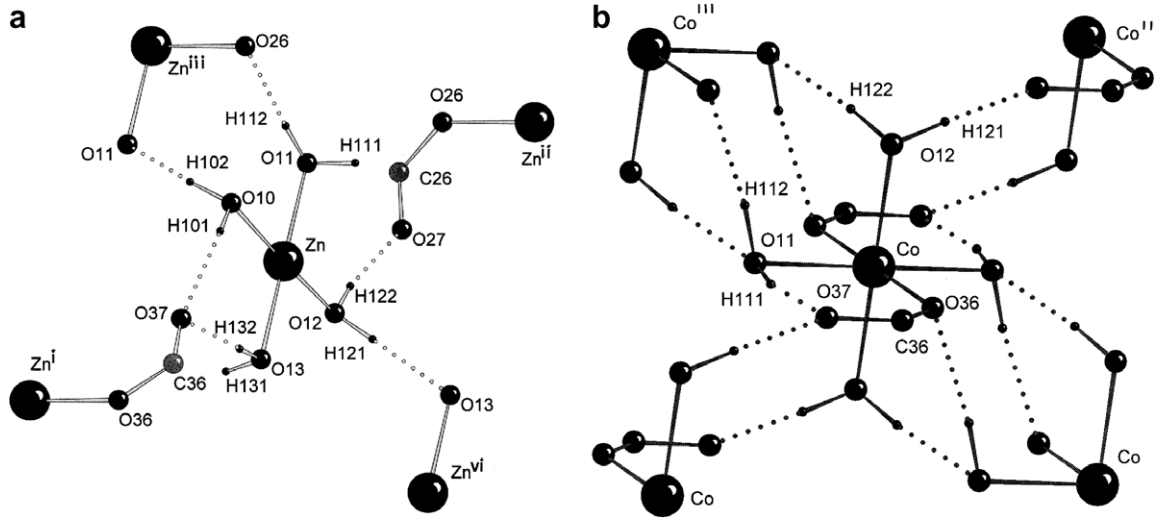

Fig. 9. Packing of $(C_7H_4NO_5)_2Zn(H_2O)_4$ (**1**) (a) and $(C_7H_4NO_5)_2Co(H_2O)_4$ (**2**) (b) concentrating on the 3D arrangement of the metal atoms. Hydrogen bonds are symbolized by dashed lines. Metal–metal distances for Zn–Zn^{iii}: 4.904 Å, Zn–Zn^{vi}, 5.200 Å and Zn–Zn^{i} = Zn–Zn^{ii}, 6.209 Å. Symmetry codes: i: $x+1$, y, z; ii: $x-1$, $y+z$; iii: $-x$, $-y$, $-z+1$; vi: $-x$, $-y+1$, $-z+1$. Metal–metal distances for Co–Co^{iii}: 5.047 Å and Co–Co^{ii}, 6.197 Å. Symmetry codes: iii: $-x+1$, $-y+1$, $-z+1$; ii: x, $y-1$, z.

crystal. Secondly, at very low temperature (3–2 K) the experimental values becomes lower than the theoretical curve showing that a weak antiferromagnetic interaction is also present in **2**. These results are in agreement with the two first levels of hydrogen bonds network in Co-complex **2** (Fig. 9b). On this basis, one can conclude that, magnetically, the cobalt ions are ferromagnetically coupled through the hydrogen bonds network of water molecules (Co^{iii}–O_{11}–O_{10}–Co, Co–Co = 5.047 Å) forming 1D ferromagnetic chains which are antiferromagnetically coupled by the hydrogen bonds developed through the *ortho*-nitrophenol groups of 3-nitro-4-hydroxybenzoate ligand.

3.5. Water/1-octanol extraction experiments

Only the details of the extraction experiment involving Zn-complex **1** are given below. Similar results were obtained with Co-complex **2**. Complex **1** (306 mg, 6.1×10^{-4} mol) was dissolved in deionized water (15 ml).

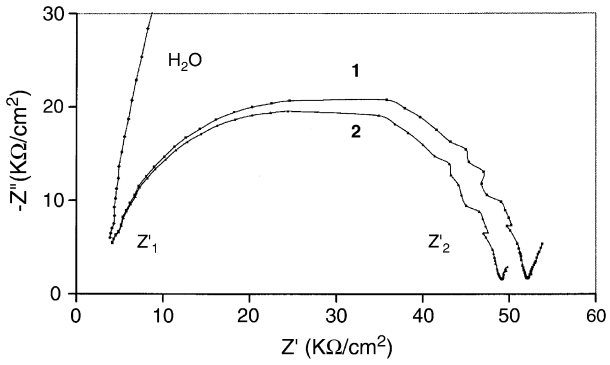

Fig. 10. Nyquist diagrams of complexes **1** and **2** at concentration of 1×10^{-4} M.

Table 5
Electrochemical conductance for complexes **1** and **2** at 20 °C[a]

Entry	Compound	Concentration (M)	Frequency (kHz)	$1/Z'$ (Ω^{-1} cm^{-1})
1	**1**	1×10^{-4}	3	2.02×10^{-5}
2	**1**	1×10^{-4}	>100	3.57×10^{-4}
3	**1**	5×10^{-4}	18	9.90×10^{-5}
4	**1**	5×10^{-4}	>100	4.54×10^{-4}
5	**2**	1×10^{-4}	3	2.16×10^{-5}
6	**2**	1×10^{-4}	>100	3.33×10^{-4}
7	**2**	5×10^{-4}	28	1.18×10^{-4}
8	**2**	5×10^{-4}	>100	3.57×10^{-4}
9	Deionized water		0.01	8.35×10^{-7}
10	Deionized water		18	2.22×10^{-4}
11	KCl	1×10^{-4}	1.4	1.47×10^{-5}
12	KCl	5×10^{-4}	0.12	7.98×10^{-5}

[a] Cell constant = 0.973.

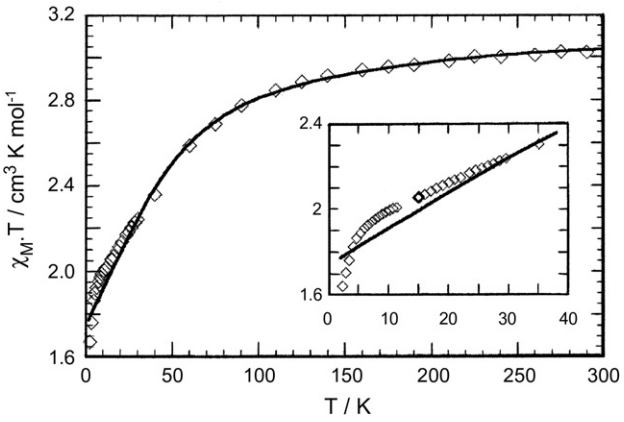

Fig. 11. $\chi_M T$ vs. T plot of Co-complex **2**, experimental (◇) and calculated (——). The inset shows the deviation of the experimental $\chi_M T$ values from the Co monomer behavior.

This solution was extracted with 1-octanol (15 ml) at room temperature. The extraction was repeated four times and the 1-octanol extracts combined. After removal of 1-octanol by vacuum distillation at 1 Torr, 3-nitro-4-hydroxybenzoic acid (111 mg, 6.1×10^{-4} mol), compound **C** in Fig. 12, was obtained as a pale yellow solid, which was unambiguously identified by comparison with an authentic sample using R_f values in thin layer chromatography and IR, UV, and ^{1}H NMR spectra. During this experiment, the color of the aqueous phase changed from pale yellow to bright orange. Evaporation of this solution at room temperature under vacuo gave a microcrystalline orange solid which was successively washed with THF and diethyl ether. Elemental analysis of this solid (Found: C, 30.71; H, 2.41; N, 5.05; Zn, 22.99%) is consistent with the molecular formula $C_7H_3NO_5Zn(H_2O)_2$ (Calc: C, 29.79; H, 2.48; N, 4.96; Zn, 23.14%) corresponding to a salt of type **D** (Fig. 12) in which the ligand **C** and Zn atom components are in the ratio of 1 to 1 (while starting complex **1** comprises two ligands **C** per Zn atom). Two water molecules are linked to each Zn atom of this salt, in order to satisfy the tetrahedral coordination of the metal. The IR spectrum of this salt, (neat, cm^{-1}): 3226 (m, ν O–H), 1596 (s, ν_{as} COO$^-$), 1518 (s), 1391 (s, ν_s COO$^-$), 1324 (s), 1248 (s), 1192 (m), 1153 (s), 1073 (m), 927 (m), 831 (m), 783 (s), 763 (s), 709 (s), 643 (s), is in agreement with the proposed molecular structure. The above outcome can be interpreted on the basis of the putative two-step equilibrium of complexes **1** and **2** in aqueous medium depicted in Fig. 12. The first step of this process involves the dissociation of the complexes into cation **A** and anion **B** [16] (note that similar discrete ionic entities were found in the crystal structures of 5(nsa)-metal complexes **3** and **4**, regioisomers of **1** and **2**, respectively, see Fig. 13). These, in turn, may interconvert through proton transfer into ligand **C** and salt **D** (in which each metal atom is coordinated to two ligand molecules acting as bidendate linkers through their carboxylato and phenoxo groups). Because of its marked lipophilicity (calculated $\log P = 1.78$) [17], ligand **C** is extractable with 1-octanol (an operation that drives the equilibrium towards **C** and **D** partners), while hydrophilic salt **D** remains in the aqueous phase.

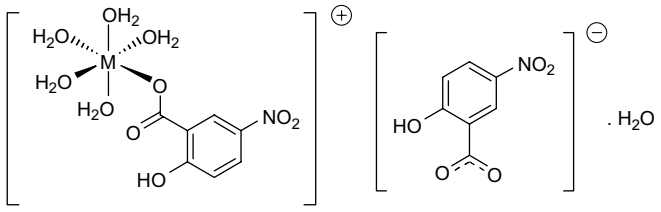

Fig. 13. Crystal structure-based canonical representation of $[M(H_2O)_5(5\text{-nsa})]^+(5\text{-nsa})^- \cdot H_2O$ (**3**, M = Zn; **4**, M = Co; **5**, M = Ni; **6**, M = Mg) [5].

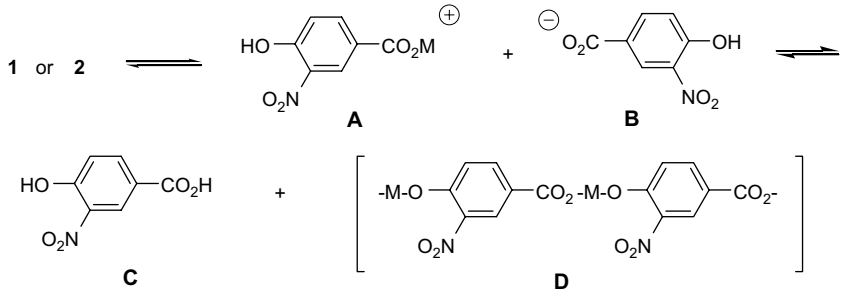

Fig. 12. Putative equilibrium of complexes **1** and **2** in aqueous solution (M = Zn or Co). The water molecules coordinated to the metal atoms have been omitted for clarity.

Table 6
Comparative anticonvulsant activities and Rotorod toxicity for complexes **1** to **6** (μmol/kg of body mass)

Compound [Reference]	MES[a]	Minimal clonic seizure[b]	scMET[c]	Rotorod toxicity[d]
1 [this work]	I at 600 ip^m at 0.5 h	A at 198 ip^m at 0.25 h	A at 198 ip^m at 0.25 h	A at 700 ip^m at 1 h
2 [this work]	I at 610 ip^m at 0.5 h	A at 200 ip^m at 1 h	A at 200 ip^m at 0.5 h	A at 610 at 0.5 h
3 [5]	I at 560 ip^m at 0.5 h	A at 185 at 0.25 h	A at 185 ip^m at 1 h	A at 185 ip^m at 0.25 h
4 [5]	A at 93 o^r at 0.25 h	A at 185 ip^m at 2 h	I at 560 ip^m at 4 h	A at 185 ip^m at 0.5 h
5 [5]	I at 570 ip^m at 4 h	A at 57 ip^m at 1 h	I at 570 ip^m at 4 h	A at 57 ip^m at 0.5 h
6 [5]	I at 600 ip^m at 4 h	A at 199 ip^m at 0.5 h	I at 600 ip^m at 4 h	I at 600 ip^m at 4 h

[a] MES = maximal electroshock seizure test.
[b] Psychomotor seizure or minimal clonic seizures are usually produced with the delivery of 6 Hz (32 mA) or slightly higher current designed to detect compounds that are missed with the MES tests which employs a larger current of 50 mA. It is a much less intense stimulation of the CNS than the MES test.
[c] scMET = subcutaneous Metrazol seizure threshold test, and Rotorod toxicity test.
[d] Rotorod toxicity, an inability to grasp the rotating rod, may be due to CNS depression due to sedative and/or hypnotic activities, or a state of eminent death, due to medullary paralysis at high doses, a common unwanted side effect caused by high doses of all anticonvulsant drugs. A = Activity at indicated dose and time of challenge. I = Inactive, ip = intraperitoneal, o = oral, m = mice, r = rats.

3.6. Anticonvulsant activities

Anticonvulsant activities for compounds **1** and **2**, as well as related (5-nitrosalicylato)–metal complexes [5] (compounds **3**–**6**, Fig. 13), are presented in Table 6.

Only **4** was found to have activity against MES-induced seizures. This modest activity was observed at a relatively low and non-toxic dose given orally to rats. Compounds **1**–**6** had activity in protecting against the less intense minimal clonic seizure with an apparent activity order being $\mathbf{5} > \mathbf{2} \cong \mathbf{1} > \mathbf{3} \cong \mathbf{6}$ and **4**, based upon these preliminary results. Only compounds **1**, **2**and **3** afforded some protection against the MET-induced seizure and the relative order of effectiveness was $\mathbf{1} > \mathbf{2} > \mathbf{3}$.

4. Conclusion

We have shown that the individual subunits of the (3-nitro-4-hydroxybenzoato) complexes of Zn(II) (**1**) and Co(II) (**2**) self-assemble via extensive hydrogen bonding involving water molecules leading to a 3D supramolecular architecture. The electrochemical impedance measurements show that these complexes are strong electrolytes in dilute aqueous solution. On the other hand, magnetic measurement of Co-complex indicates that the Co ions are ferromagnetically coupled thought the hydrogen bonds network of water molecules forming 1D ferromagnetic chains.

The anticonvulsant activities of complexes **1** and **2** as well as related Zn(II), Co(II), Ni(II) and Mg(II) (5-nitrosalicylato) complexes (**3**, **4**, **5** and **6**, respectively) where also determined. The pharmacological responses obtained for these complexes are consistent with those obtained for many related metal complexes [4–10].

The transport of therapeutics across the blood–brain barrier (BBB) is critical for the treatment of disorders of the central nervous system. There is a good correlation between BBB penetration *in vivo* and lipid solubility of a drug, the latter being conventionally expressed as its partition coefficient (*P*), calculated as the ratio of solubilities in 1-octanol and water [18]. Because of their marked hydrophilicity, revealed by their notable water solubility (Section 2.3) and the important conductance of their aqueous solutions (Section 3.3), metal salts **1** and **2** can have direct access to the systemic circulation *via* blood plasma. Lipophilic ligand **C**, which is in equilibrium with complexes **1** and **2** in aqueous medium (Section 3.5), can then penetrate the BBB by diffusion (passive translocation *via* a lipophilic pathway). On this basis, we may hypothesize that the active form of these anticonvulsant metal complexes might be free ligand **C**, the metal salts playing the role of hydrosoluble vectors that release the drug at BBB level. This hypothesis is in full agreement with a previous investigation of (salicylato)–copper complex equilibrium under physiological conditions, which ruled out any implication of the copper complex in the anti-inflammatory activity, since the salicylate anion cannot significantly mobilize plasma copper into tissue–diffusible complexes. Even though the salicylate ligand can effectively promote the gastrointestinal absorption of copper, the reciprocal effect of the metal upon the drug seems to be negligible, except for high metal-to-drug ratios [19–21].

Acknowledgements

Financial support of Université Paris XI, CNRS and Ecole Centrale Paris is gratefully acknowledged. The authors thank Mrs. S. Mairesse-Lebrun for performing elemental analyses. We are also thank Mr. James Stables for his assistance in obtaining data pertain to the anticonvulsant and Rotorod toxicities of our compounds *via* the DHHS, NIH, NINDS ADD program (USA).

Appendix A. Supplementary material

CCDC 647852 and 647853 contain the supplementary crystallographic data for **1** and **2**. These data can be obtained free of charge via http://www.ccdc.cam.ac.uk/conts/retrieving.html, or from the Cambridge Crystallographic Data Centre, 12 Union Road, Cambridge CB2

1EZ, UK; fax: (+44) 1223-336-033; or e-mail: deposit@ccdc.cam.ac.uk. Supplementary data associated with this article can be found, in the online version, at doi:10.1016/j.poly.2007.10.006.

References

[1] F.D. Rochon, G. Massarweh, Inorg. Chim. Acta 304 (2000) 190.
[2] S.H. Rahaman, D. Bose, H. Chowdhury, G. Mostafa, H.-K. Fun, B.K. Ghosh, Polyhedron 24 (2005) 1837.
[3] N.E. Ghermani, G. Morgant, J. d'Angelo, D. Desmaële, B. Fraisse, F. Bonhomme, E. Dichi, M. Sghaier, Polyhedron 26 (2007) 2880.
[4] J.R. J Sorenson, Free Radic. Biol. Med. 13 (1992) 593.
[5] G. Morgant, N. Bouhmaida, L. Balde, N.E. Ghermani, J. d'Angelo, Polyhedron 25 (2006) 2229.
[6] J.R.J. Sorenson, J. Med. Chem. 19 (1976) 135.
[7] J.R.J. Sorenson, Prog. Med. Chem. 15 (1978) 211.
[8] B. Viossat, J.-C. Daran, G. Savouret, G. Morgant, F.T. Greenaway, N.-H. Dung, V.A. Pham-Tran, J.R.J. Sorenson, J. Inorg. Biochem. 96 (2003) 375.
[9] P. Lemoine, B. Viossat, N.H. Dung, A. Tomas, G. Morgant, F.T. Greenaway, J.R.J. Sorenson, J. Inorg. Biochem. 98 (2004) 1734.
[10] B. Viossat, F.T. Greenaway, G. Morgant, J.-C. Daran, N.-H. Dung, J.R.J. Sorenson, J. Inorg. Biochem. 99 (2005) 355.
[11] ASTRO (5.00), SAINT (5.007) and SADABS (5.007). Data Collection and Processing Software for the SMART System (5.054). Siemens (BRUKER-AXS) Analytical X-ray Instruments Inc., Madison, WI, 1998.
[12] A. Altomare, M.C. Burla, M. Camalli, G.L. Cascarano, G. Giacovazzo, A. Guagliardi, A. Grazia, G. Moliterni, G. Polidori, R. Spagna, J. Appl. Crystallogr. 32 (1999) 115.
[13] D.J. Watkin, C.K Prout, J.R. Carruthers, P.W. Betteridge, R.I. Prout, CRYSTALS Issue 11. Chemical Crystallography Laboratory, University of Oxford, UK, 2001.
[14] D.J. Watkin, C.K. Prout, L.J. Pearce, CAMERON, Chemical Crystallography Laboratory, University of Oxford, UK, 1996.
[15] O. Kahn, Molecular Magnetism, VCH, New York, 1993.
[16] L.H.J. Lajunen, R. Portanova, J. Piispanen, M. Tolazzi, Pure Appl. Chem. 69 (1997) 329.
[17] N. Bodor, P. Buchwald, J. Phys. Chem. B 101 (1997) 3404.
[18] N.J. Abbott, I.A. Romero, Mol. Med. Today (1996) 106.
[19] V. Brumas, B. Brumas, G. Berthon, J. Inorg. Biochem. 57 (1995) 191.
[20] H. Miche, V. Brumas, G. Berthon, J. Inorg. Biochem. 68 (1997) 27.
[21] B. Halova-Lajoie, V. Brumas, M.M.L. Fiallo, G. Berthon, J. Inorg. Biochem. 100 (2006) 362.